Low-Complexity User Selection Algorithms for Multiuser Transmissions in mmWave WLANs

Khalid Aldubaikhy, *Student Member, IEEE*, Wen Wu, *Student Member, IEEE*, Qiang Ye, *Member, IEEE*, and Xuemin Shen, *Fellow, IEEE*

***Abstract*— In this paper, we propose a low-complexity user selection algorithm for an uplink multiuser transmission in millimeter wave (mmWave) WLAN. We first formulate the user selection problem, taking hybrid beamforming (HBF), an NP-hard problem, into consideration. We then develop a three-step HBF algorithm that incorporates user selection. Specifically, users can be selected based on semi-orthogonality instead of collecting perfect channel state information (CSI) from all potential users. We optimize the digital beamforming to mitigate residual interference among the selected users. Furthermore, we provide analytical validation for the proposed user selection algorithm and study the impact of angle correlation, analog beam pattern, and beamwidth on the achievable rate of the selected users. Extensive simulations validate the performance of the proposed overall HBF algorithm when compared with existing solutions.**

***Index Terms*— User selection, hybrid beamforming, mmWave, WLANs, IEEE 802.11ay, multiuser MIMO.**

I. Introduction

MILLIMETER wave (mmWave) communication technology is expected to play a crucial role in future wireless networks with large user populations because of the large spectrum band it can provide [2]–[6]. To further improve spectrum efficiency over the mmWave bands in wireless local area networks (WLANs) with a large number of users, the IEEE 802.11ay standard was developed from the traditional IEEE 802.11ad standard, aiming to support multiuser multiple-input multiple-output (MIMO). Moreover, network throughput can be improved significantly by using uplink multiuser MIMO transmission in ultra-dense networks. Although uplink multiuser transmission is a promising technology, both the user selection algorithm and the beamforming (BF) mechanism need to be considered in an mmWave system with a large user population.

Manuscript received January 9, 2019; revised June 27, 2019 and November 25, 2019; accepted December 23, 2019. Date of publication January 14, 2020; date of current version April 9, 2020. This article was presented in part at the 2018 IEEE Global Communications Conference (2018 IEEE GLOBECOM). The associate editor coordinating the review of this article and approving it for publication was A. Zaidi. *(Corresponding author: Khalid Aldubaikhy.)*

Khalid Aldubaikhy is with the Department of Electrical Engineering, Qassim University, Buraydah 52571, Saudi Arabia (e-mail: khalid@qec.edu.sa).

Wen Wu and Xuemin Shen are with the Department of Electrical and Computer Engineering, University of Waterloo, Waterloo, ON N2L 3G1, Canada (e-mail: w77wu@uwaterloo.ca; sshen@uwaterloo.ca).

Qiang Ye is with the Department of Electrical and Computer Engineering and Technology, Minnesota State University, Mankato, MN 56001, USA (e-mail: qiang.ye@mnsu.edu).

Color versions of one or more of the figures in this article are available online at http://ieeexplore.ieee.org.

Digital Object Identifier 10.1109/TWC.2020.2964551

User selection in large-scale multiuser MIMO is crucial due to the multiuser interference and the potential collection of channel state information (CSI) to find the best group of users [7], [8]. In particular, the orthogonality of the instantaneous channels among selected users can affect their achievable rates where the users are coupled [9]–[12]. The literature uses several criteria for user selection or user grouping to solve the problem of selecting a subset of users. An explicit way to solve the problem is to find an optimal subset of users by deploying an exhaustive search over all users. However, in dense deployment scenarios, this requires formidable CSI overhead, and its complexity can grow significantly with the number of users. Other criteria [9]–[11] are used to simplify the user selection problem into sub-optimal algorithms by utilizing the orthogonality criterion as a selection metric, such as the largest principal angle [13], subspace collinearity [14] and chordal distance [15]. Thus, user selection is essential in multiuser MIMO, especially when the number of users is large.

Employing traditional digital BF in an mmWave system is challenging due to high feedback overhead and the power consumption of the mixed signal processing components [16], [17]. A potential solution is to exploit the concept of hybrid beamforming (HBF) in the mmWave systems by combining analog BF and digital BF. The literature proposes several approaches that split the BF process into two stages, analog BF and digital BF optimization, to simplify finding a jointly optimal solution in the HBF [17]–[22]. In [22], a two-stage HBF algorithm is developed, with the minimum mean square error approach employed for the digital BF stage while the Gram-Schmidt approach is used for the analog BF stage. In [21], a two-stage HBF algorithm is also considered, using a one-bit analog-to-digital converters (ADCs) approach to reduce the power consumption of the ADCs in the mmWave system. In [19], an HBF algorithm is proposed in which a mean square error measure and an orthogonal matching pursuit approach are adopted for the digital BF and analog BF, respectively. In [20], an HBF joint optimization process is adopted, with the analog phase shifter, transmit power, and receive antenna selection matrix considered in the HBF joint optimization problem.

However, the existing HBF algorithms do not consider the user selection algorithm, even though the user selection needs to be jointly considered with the HBF algorithm when there are a high number of users. Thus, computational complexity can be significant in dense deployment scenarios. Specifically,

there can be high power consumption due to the increased demand for radio frequency (RF) chains, with the number of simultaneous transmissions limited to the RF chain number. The assumption that the system can serve users up to the total number of RF chains without considering user selection to maximize the data rate is not realistic in an mmWave system with a large number of users. Also, CSI acquisition overhead from all the potential users can be considerable. Even though there have been substantial research efforts on existing HBF algorithms, to the best of our knowledge, the user selection algorithm in dense user scenarios has not been incorporated into the HBF algorithm for uplink multiuser MIMO mmWave systems.

In this paper, we aim to address this limitation by proposing a three-step HBF algorithm that considers the user selection problem. The proposed algorithm can achieve simultaneous uplink transmissions when the number of users is large while keeping the computational complexity as low as possible. This paper offers three main contributions:

1) We develop a three-step HBF algorithm, overall-HBF, to combine user selection with the HBF algorithm while keeping the computational complexity low. Specifically, we propose a low-complexity user selection algorithm in which semi-orthogonality is exploited as a selection metric based on analog BF information rather than seeking full CSI from all users. In addition, we optimize the digital BF by maximizing the signal-to-interference-plus-noise ratio (SINR) to further enhance system performance instead of utilizing the traditional zero-forcing (ZF) method.
2) We analyze the influence of angle correlation, analog beam pattern, and beamwidth on the proposed user selection algorithm. We then determine the computational complexity of the proposed algorithm as compared to the optimal user selection solution.
3) We evaluate the energy efficiency of the proposed overall-HBF algorithm and examine the effect of RF-chain implementation. We carry out extensive simulations to validate the performance of the proposed algorithm with respect to both energy efficiency and the average sum rate of the system, as compared to the existing HBF algorithms.

The remainder of this paper is organized as follows. We first provide the system model in Section II. Then, we describe the proposed overall-HBF algorithm in Section III. We discuss the performance analysis of the proposed user selection in Section IV. We present simulation results in Section V, followed by conclusions in Section VI.

Notations: Boldface upper-case letters are used for matrices, while boldface lower-case letters are used for vectors. The transpose, Hermitian, and inverse of a matrix $\mathbf{A}$ are denoted by the superscript $\mathbf{A}^T$, $\mathbf{A}^H$, and $\mathbf{A}^{-1}$, respectively. The notations $\mathcal{CN}(\cdot,\cdot)$ and $\mathcal{N}(\cdot,\cdot)$ represent the complex circular and real normal distribution, respectively. An identity matrix of size $n \times n$ is denoted by $\mathbf{I}_n$, and a dimensional complex space of size $m \times n$ is denoted by $\mathbb{C}^{m\times n}$. The expectation of $\mathbf{A}$ is denoted by $\mathbb{E}[\mathbf{A}]$.

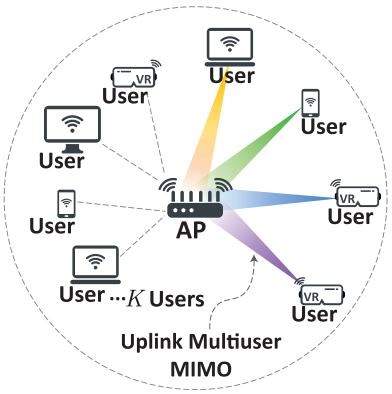

Fig. 1. Network model.

TABLE I
SUMMARY OF MAIN ACRONYMS

Acronyms	Description
ATI	Announcement transmission interval
A-BFT	Associated beamforming training
BI	Beacon interval
BTI	Beacon transmission interval
BF	Beamforming
CSI	Channel state information
DTI	Data transmission interval
DMG	Directional multi-gigabit
HBF	Hybrid beamforming
I-TXSS	Initiator transmit sector sweep
R-TXSS	Responder transmit sector sweep
SP	Scheduled-service period
SID	Sector identification
SLS	Sector level sweep
SSW	Sector sweep
VS	Virtual sector

II. System Model

We use the IEEE 802.11ay mmWave system architecture to describe the uplink multiuser MIMO BF problem, while achieving backward compatibility with traditional IEEE 802.11ad. As shown in Fig. 1, simultaneous uplink transmissions are considered in this model, with the benefits of the spatial dimension of the channel applied by using the physical layer mechanism of the multiuser MIMO. In this scenario, we consider one access point (AP) and K users. The AP and users are all equipped with steerable directional antennas and can use enhanced-directional multi-gigabit (DMG), as defined in IEEE 802.11ay. Table I summarizes the acronyms used hereinafter.

A. IEEE 802.11ay Analog BF Training

Fig. 2 shows the beacon interval (BI) of the directional medium access control (MAC) of IEEE 802.11ay. Each BI consists of four main access periods: the beacon transmission interval (BTI), association beamforming training (A-BFT), announcement transmission interval (ATI), and data transfer interval (DTI). BF training for the 802.11ay is similar to the

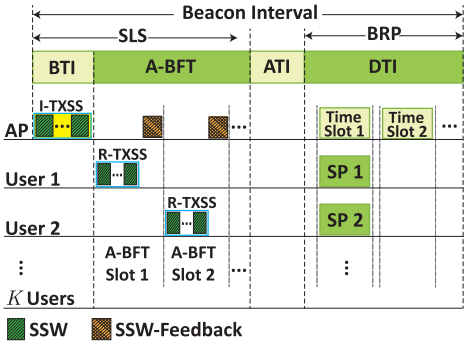

Fig. 2. The analog BF training MAC protocol of the IEEE 802.11ay.

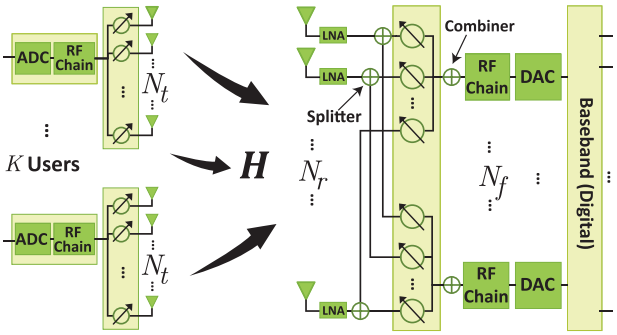

Fig. 3. HBF architecture.

legacy 802.11ad but includes new BF training stages, such as single-user MIMO BF and multiuser MIMO BF, to enhance the BF process [23]. The analog BF training for the IEEE 802.11ay is divided into two main stages, the sector level sweep (SLS) and the beam refinement protocol (BRP). The BF training is first done in the SLS and can then be performed again with an optional iterative BF process in the BRP. The BF process of the SLS stage is illustrated in the following three steps:

1) The AP transmits sector sweep (SSW) frames in the initiator transmit sector sweep (I-TXSS) phase of the BTI, using multiple DMG Beacon frames with different sector beams (multiple sectors in different directions); each user receives these frames in the quasi-omni mode.
2) During A-BFT, each user transmits SSW frames with different sector beams in the responder transmit sector sweep (R-TXSS) phase for association with the AP, and the AP receives these SSW frames in the quasi-omni mode. During this process, information about the best sector identification (SID) of the AP (which means the best sector beam) is transmitted in each SSW frame.
3) The AP feeds the best SID, i.e., that with the highest signal-to-noise ratio (SNR), to every associated user during the SSW-Feedback frame by using the best SID from the previous step.

Then, the AP allocates the selected users during the ATI by using the scheduled-service period (SP) time slots. Data transmission frames are sent during the DTI period by allocating the SPs or contention-based access periods (CBAPs). This paper only considers SP allocation, and we assume that the length of the transmission frames during the DTI is equal.

B. HBF Model

We consider an uplink multiuser HBF system for a subset of users. The AP is equipped with N_r antennas, and each user is equipped with N_t antennas, as shown in Fig. 3. We assume there are N_f RF chains at the AP, to support multiple users simultaneously, while a single RF chain is available for each user. We assume that the number of users, K, is larger than the number of available RF chains at the AP, N_f ($K \gg N_f$). User selection is necessary because the HBF approach requires a limited number of RF chains at the AP to reduce complexity and power consumption. Let $\mathcal{K} = \{1, ..., K\}$ be the set of all potential users, and $\mathcal{S} \subseteq \mathcal{K}$ be the subset of selected users served by the AP simultaneously. For ease of representation, let S be the cardinality of the subset $\mathcal{S}$ ($S = |\mathcal{S}|$).

Both AP and user are assumed to use predefined analog beams due to the constraints of the RF hardware: the RF phase shifters can take only quantized angles. Thus, the analog BF vector at the i-th user is represented by $\mathbf{u}_i \in \mathbb{C}^{N_t \times 1}$, where $\mathbf{u}_i$ is an element of the analog transmitter BF vectors $\mathcal{F}_t$ with quantized phases and constant magnitude items. Similarly, the analog BF vector at the i-th RF chain at the AP is denoted by $\mathbf{v}_i \in \mathbb{C}^{N_r \times 1}$, where $\mathbf{v}_i$ is an element of the analog receiver BF vectors $\mathcal{F}_r$. We assume that each user is transmitting a single uplink data stream. Therefore, the transmitted signal of the i-th user is

$$\mathbf{s}_i = \sqrt{P}\mathbf{u}_i x_i, \tag{1}$$

where x_i and P are, respectively, the data symbol and transmit power for the i-th user, such that $\mathbb{E}[x_i] = 0$ and $\mathbb{E}[|x_i|^2] = 1$. To simplify analysis, we assume all users employ the same transmit power [17], [20]. For traceability, we also assume a block-fading channel model, in which the AP observes the received signal as

$$\mathbf{r} = \sum_{i=1}^{S} \sqrt{P}\mathbf{H}_i \mathbf{u}_i x_i + \mathbf{n}, \tag{2}$$

where $\mathbf{H}_i \in \mathbb{C}^{N_r \times N_t}$ is the channel matrix from the i-th user to the AP, and $\mathbf{n} \in \mathbb{C}^{N_r \times 1}$ is the additive white Gaussian noise vector at the AP, with zero mean and variance per element σ^2.

The mmWave MIMO channel can be illustrated using the broadly applicable Saleh-Valenzuela model [24] with L limited scatters in user i's channel. Therefore, we adopt this model to construct the uplink channel matrix $\mathbf{H}_i$ from the i-th user to the AP:

$$\mathbf{H}_i = \sqrt{\frac{N_t N_r}{L_i}} \sum_{l=1}^{L_i} g_{i,l} \mathbf{a}_r(\theta_{i,l}) \mathbf{a}_t(\phi_{i,l})^H, \tag{3}$$

where $\mathbf{a}_t(\phi_{i,l})$ and $\mathbf{a}_r(\theta_{i,l})$ are the antenna array response vectors for the i-th user and the AP, respectively. $\theta_{i,l}$ and $\phi_{i,l} \in [0, 2\pi]$ denote the angles of arrival and departure, respectively, of the l-th path. $g_{i,l}$ denotes the channel gain of the l-th path. A uniform linear array (ULA) is adopted in this paper even though our algorithms and results can be revised

to work with other antenna arrays. Thus, the $\mathbf{a}_t(\phi_{i,l})^H$ and $\mathbf{a}_r(\theta_{i,l})$ can be written as

$$\mathbf{a}_r(\theta_{i,l}) = \frac{1}{\sqrt{N_r}}[1, e^{j\frac{2\pi}{\lambda}d\sin(\theta_{i,l})}, \ldots, e^{j(N_r-1)\frac{2\pi}{\lambda}d\sin(\theta_{i,l})}]^T, \tag{4}$$

$$\mathbf{a}_t(\phi_{i,l}) = \frac{1}{\sqrt{N_t}}[1, e^{j\frac{2\pi}{\lambda}d\sin(\phi_{i,l})}, \ldots, e^{j(N_t-1)\frac{2\pi}{\lambda}d\sin(\phi_{i,l})}]^T, \tag{5}$$

where $d = \lambda/2$ denotes the distance between antenna elements and λ represents the mmWave signal wavelength.

We consider a unitary Discrete Fourier Transform (DFT) codebook similar to that in the IEEE 802.11ad/ay standard to define $\mathcal{F}_t$ and $\mathcal{F}_r$. The analog BF codebooks are given by

$$\mathcal{F}_t = [\mathbf{a}_t(\delta_1),\ \mathbf{a}_t(\delta_2),\ \cdots\ \mathbf{a}_t(\delta_{N_t})], \tag{6}$$

$$\mathcal{F}_r = [\mathbf{a}_r(\zeta_1),\ \mathbf{a}_r(\zeta_2),\ \cdots\ \mathbf{a}_r(\zeta_{N_r})], \tag{7}$$

where the angles δ_i satisfy $\frac{2\pi d}{\lambda}sin(\delta_i) = \frac{2\pi i}{N_t}\ \forall i = 1, 2, \ldots N_t$, and the angles ζ_i satisfy $\frac{2\pi d}{\lambda}sin(\zeta_i) = \frac{2\pi i}{N_r}\ \forall i = 1, 2, \ldots N_r$ [17], [23], [25]. The elements of each codebook indicate the steering angles (or sectors).

The signal received after multiplying by the analog BF matrix at the AP can be expressed by

$$\begin{aligned}\mathbf{y} &= \mathbf{V}^H\mathbf{r},\\ &= \mathbf{V}^H\sum_{i=1}^{S}\sqrt{P}\mathbf{H}_i\mathbf{u}_i x_i + \mathbf{V}^H\mathbf{n},\\ &= \sqrt{P}\mathbf{V}^H\mathbf{H}_i\mathbf{u}_i x_i + \underbrace{\sqrt{P}\sum_{j\neq i}^{S}\mathbf{V}^H\mathbf{H}_j\mathbf{u}_j x_j}_{\text{interference}} + \mathbf{V}^H\mathbf{n},\end{aligned} \tag{8}$$

where $\mathbf{V} = [\mathbf{v}_1, \mathbf{v}_2, \ldots, \mathbf{v}_S]$ is the analog BF matrix comprised of S analog BF vectors, and $\mathbf{V}^\mathbf{H}\mathbf{V} = \mathbf{I}$. The multiuser interference generated by $S-1$ transmitting users is demonstrated in the second item of (8). Note that for simplicity, the successive interference canceling (SIC) in our work is not assumed.

Digital BF is then employed to mitigate the multiuser interference. Let $\mathbf{F} = [\mathbf{f}_1, \mathbf{f}_2, \ldots, \mathbf{f}_S] \in \mathbb{C}^{S\times S}$ be the digital BF at the AP such that $\|\mathbf{f}_i\|^2 = 1$. Then, $\mathbf{f}_i$ is utilized to decode x_i for the i-th user. Thus, the decoded symbol can be expressed as

$$\hat{x} = \sqrt{P}\mathbf{f}_i^H\mathbf{V}^H\mathbf{H}_i\mathbf{u}_i x_i + \underbrace{\sqrt{P}\sum_{j\neq i}^{S}\mathbf{f}_i^H\mathbf{V}^H\mathbf{H}_j\mathbf{u}_j x_j}_{\text{interference}} + \mathbf{f}_i^H\mathbf{V}^H\mathbf{n}. \tag{9}$$

Given the decoded symbol at the AP in (9), the SINR of the i-th user is given by

$$\gamma_i = \frac{P|\mathbf{f}_i^H\mathbf{V}^H\mathbf{H}_i\mathbf{u}_i|^2}{P|\sum_{j\neq i}^{S}\mathbf{f}_i^H\mathbf{V}^H\mathbf{H}_j\mathbf{u}_j|^2 + \sigma^2}. \tag{10}$$

Thus, the achievable rate for the i-th user can be written as

$$R_i = \log_2\left(1 + \frac{P|\mathbf{f}_i^H\mathbf{V}^H\mathbf{H}_i\mathbf{u}_i|^2}{P|\sum_{j\neq i}^{S}\mathbf{f}_i^H\mathbf{V}^H\mathbf{H}_j\mathbf{u}_j|^2 + \sigma^2}\right). \tag{11}$$

C. Problem Formulation

The sum rate (R_{sum}) of the uplink multiuser network can be maximized. The optimal HBF can be determined by finding the optimal analog BF, optimal digital BF, and optimal subset of users. The optimization problem can be formulated as

$$\mathcal{P}1: \max_{\mathbf{U},\mathbf{V},\mathbf{F},\mathcal{S}} R_{sum} = \sum_{i=1}^{S} R_i \tag{12a}$$

$$\text{s.t. } \mathbf{u}_i \in \mathcal{F}_t, \quad \forall i \in \mathcal{S}, \tag{12b}$$

$$\mathbf{v}_i \in \mathcal{F}_r, \quad \forall i \in \mathcal{S}, \tag{12c}$$

$$\|\mathbf{f}_i\|^2 = 1, \quad \forall i \in \mathcal{S}, \tag{12d}$$

$$\mathcal{S} \subseteq \mathcal{K}, \tag{12e}$$

$$|\mathcal{S}| \leq N_f. \tag{12f}$$

The optimization problem ($\mathcal{P}1$) is a mixed integer programming problem. This is a non-convex NP-hard problem, and finding the optimal solution is neither practical nor tractable for the following reasons: (i) constraints (12b) and (12c) are finite sets with integer constraints; (ii) due to the interference, the objective function is still a non-convex function of digital BF vectors $\mathbf{f}_i$, even though the analog BF vectors are fixed; (iii) to find the optimal subset of users that will maximize the sum rate, the subset of users needs to be jointly selected with both analog BF and digital BF; this means an exhaustive search over all K users is required, which can lead to high computational complexity: high CSI acquisition overhead is needed at the AP to collect CSI from all potential users in order to identify the best user group.

The problem of finding joint optimal analog BF and digital BF (similar to $\mathcal{P}1$) has been studied before, in [17], [19], [20], [22]. However, the user selection problem has not been considered with the HBF algorithm when the number of users is larger than that of available RF chains. To solve the challenges associated with the user selection problem, we propose a novel overall-HBF algorithm with a low-complexity user selection algorithm in Section III. The aim of our proposed algorithm is to incorporate the user selection algorithm into the HBF algorithm while keeping computational complexity low and realizing satisfactory performance.

III. Overall-HBF Algorithm

To reduce the high computational complexity associated with solving problem $\mathcal{P}1$, and to consider the user selection problem when $K \gg N_f$, we employ a suboptimal three-step algorithm, summarized in Algorithm 1.

The analog BF, digital BF, and user selection are separately designed in the proposed overall-HBF algorithm. First, the AP and each user maximize their anticipated beam steering between one another using the analog BF, without considering the multiuser interference. This step adopts the SLS BF training of the IEEE 802.11ay. Second, a user selection algorithm selects a subset of users based only on the information from the analog BF training realized in the first step. Thus, no additional full CSI feedback is required. Third, the final step adopts digital BF to mitigate the residual multiuser interference, using an SINR maximization method.

Algorithm 1 Overall-HBF Algorithm

Inputs: $\mathcal{F}_t$ and $\mathcal{F}_r$, the codebook sets of analog BF for each user and AP, respectively.

Outputs: $\mathbf{u}_i$, $\mathbf{v}_i$, $\mathbf{f}_i$, and $\mathcal{S}$.

First Step: Analog BF

Each user and AP selects $\mathbf{u}_i$ and $\mathbf{v}_i$ to determine the best beam pair, as in $\mathcal{P}2$. Then, the best SID pair is obtained through the sequential training method using SLS BF.

Second Step: Proposed User Selection

The AP divides the coverage area into virtual sectors (VSs).

The VSs are divided into two semi-orthogonal groups: VG_{g1} and VG_{g2}.

The AP selects a subset of users based on the best SID reported in step 1.

The AP schedules multiuser transmission in separate time slots for each group.

Third Step: Digital BF

The AP estimates the effective channel, $\bar{\mathbf{h}}_i = \mathbf{V}^H \mathbf{H}_i \mathbf{u}_i, \forall i \in \mathcal{S}$, for each user$_i$.

The AP designs $\mathbf{f}_i$ in (18) for the i-th RF chain, with all effective CSI.

The AP normalizes $\mathbf{f}_i = \frac{\mathbf{f}_i}{\|\mathbf{f}_i\|}$ for i.

A. First Step: Analog BF

The SLS BF training of the IEEE 802.11ay standard is utilized to represent the analog-beam-pattern (analog BF). Analog BF vectors can only take finite values because of RF hardware constraints: the RF phase shifters only take quantized angles. The analog BF vectors can be selected from finite-size codebooks in (6) and (7), with both the AP and users selecting from these predefined analog beams.

Each user and AP has to choose $\mathbf{u}_i \in \mathcal{F}_r$ and $\mathbf{v}_i \in \mathcal{F}_t$, the analog BF codebooks, to maximize channel gain and determine the best transmit and receive beam pair for each user:

$$\mathcal{P}2: \max_{\mathbf{u}_i, \mathbf{v}_i} \|\mathbf{v}_i^H \mathbf{H}_i \mathbf{u}_i\|^2 \tag{13a}$$

$$\text{s.t. } \mathbf{u}_i \in \mathcal{F}_t, \quad \forall i \in \mathcal{K} \tag{13b}$$

$$\mathbf{v}_i \in \mathcal{F}_r, \quad \forall i \in \mathcal{K} \tag{13c}$$

An exhaustive search method requiring a search over the entire $\mathcal{F}_t \times \mathcal{F}_r$ of possible transmit and receive steering angles combinations (analog BF vectors combinations) can solve the above problem. However, this can increase analog BF training overhead significantly. The IEEE 802.11ad/ay standards use SLS BF training to handle this and reduce the latency.

In this step, we adopt the SLS BF training in IEEE 802.11ad/ay. Since we use iterative bidirectional training with sequential time slots, the full CSI is not required. The SLS BF training can determine the best SID pair in the sequential training method, as explained in Subsection II-A.

B. Second Step: Proposed User Selection Algorithm

In order to reduce computational complexity, the user selection algorithm is performed independently in the second step of the overall-HBF algorithm after analog BF training is completed. The proposed user selection does not require full CSI; it can be realized from only the analog BF information.

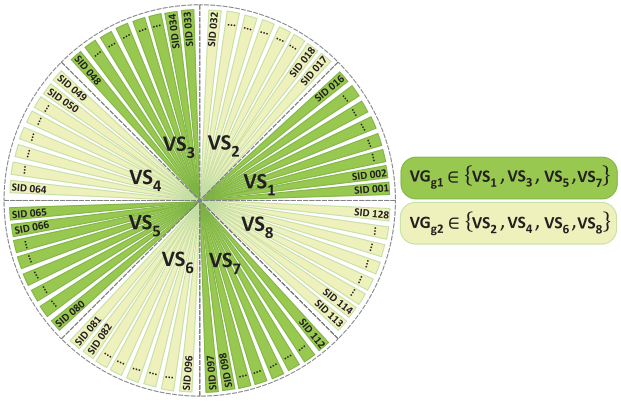

Fig. 4. The SID and the user selection algorithm concept when $A = 8$ and $p = 128$.

As shown in Fig. 4, we propose a user selection algorithm to divide users into two semi-orthogonal groups without the need to find an optimal set of users by collecting the CSI for all users. The coverage area is divided into VSs ($A = 8$ in the example in Fig. 4) and these sectors are further divided into two semi-orthogonal groups, VG_{g1} and VG_{g2}, such that multiuser transmission can be attained in separate time slots for each group. Divisions are based on the beam direction associated with the optimal SID, determined when the users report their SID during analog BF training. Therefore, to calculate the number of SIDs per VG_{g1} or VG_{g2}, groups VG_{g1} and VG_{g2} can be formulated as $\left(\frac{A+2pq-2p}{A}\right) \leq \text{SID} \leq \left(\frac{2pq-p}{A}\right)$ and $\left(\frac{A+2pq-2p}{A}\right) \leq \text{SID} \leq \left(\frac{2pq-p}{A}\right)$, respectively, where A is the total number of VSs, p is the total number of SIDs, and $q = \{1, 2, ..., A/2\}$. The details of the proposed user selection algorithm are shown in Algorithm 2.

Note that when more than one user is reported in the same VS, only the user with the highest SNR is selected for multiuser transmission. While we use the SNR reported during A-BFT as a selection metric, any other scheduling mechanism could be utilized. The details of the proposed user selection algorithm are as follows:

1) After the BF training is completed, the AP checks and examines the best SID information exchanged by all associated users.
2) If the best SID of the i-th user belongs to VG_{g1} or VG_{g2}, then the i-th user is selected and scheduled for simultaneous transmission at time slot t or $t+1$, respectively.
3) If there is more than one user in any VSs of VG_{g1} or VG_{g2}, then only the one user with the highest SNR is selected.
4) The unselected users are re-evaluated for simultaneous transmission by the algorithm until no user can be selected for VG_{g1} or VG_{g2}. Then, the AP schedules the unselected users in different time slots sequentially (not simultaneous transmission).

Algorithm 2 Proposed User Selection Algorithm

Input: The best SID information for each user.
Repeat
  for *SID* $= 1$ *to* p **do**
    if *the best SID of the* i*-th user belongs to* VG_{g1} $\left\{\left(\frac{A+2pq-2p}{A}\right) \leq SID \leq \left(\frac{2pq-p}{A}\right)\right\}$ **then**
      select user$_i$ and assign them to $\mathcal{S}$ at time slot t
    end
    if *more than one user in the VSs of* VG_{g1} **then**
      select only the one user with the highest SNR
    end
    if *the best SID of the* i*-th user belongs to* VG_{g2} $\left\{\left(\frac{A+2pq-p}{A}\right) \leq SID \leq \left(\frac{2pq}{A}\right)\right\}$ **then**
      select user$_i$ and assign them to $\mathcal{S}$ at time slot $t+1$
    end
    if *more than one user in the VSs of* VG_{g2} **then**
      select only the one user with the highest SNR
    end
  end
Until there are no more users that can be selected **then** the AP schedules the unselected users sequentially in advanced sequential time slots t.

C. Third Step: Digital BF Approach

After determining the subset of users ($\mathcal{S}$) in the second step of the overall-HBF algorithm, the AP can obtain digital BF vectors in order to cancel the remaining multiuser interference from the selected users. By the time the second and third steps are complete, the AP is ready to simultaneously serve the selected users in $\mathcal{S}$ at each time slot (t). The interference mitigation of the ZF method, a common approach to digital BF, comes at the expense of energy inefficiency. Uplink scenarios should use an energy-efficient digital BF method because of limited power resources, e.g., on-board battery power. Therefore, we use an SINR maximization method instead of the more conventional ZF method in the digital BF step in order to increase energy efficiency.

For simplicity, let $h_{i,j} = \mathbf{v}_j^H \mathbf{H}_i \mathbf{u}_i \in \mathbb{C}^{1\times 1} \forall i \in \mathcal{S}$ be the effective channel gain between the i-th user and j-th RF chain at the AP. Furthermore, let $\bar{\mathbf{h}}_i = \mathbf{V}^H \mathbf{H}_i \mathbf{u}_i \in \mathbb{C}^{S\times 1}$ be the effective channel vector between the i-th user and the AP. Then, the SINR in (10) can be written as

$$\gamma_i = \frac{|\mathbf{f}_i^H \bar{\mathbf{h}}_i|^2}{|\mathbf{f}_i^H (\sum_{j\neq i}^{S} \bar{\mathbf{h}}_j + \frac{1}{\sqrt{P}}\bar{\mathbf{n}})|^2}, \tag{14}$$

where $\bar{\mathbf{n}} \triangleq \mathbf{V}^H \mathbf{n} \in \mathbb{C}^{S\times 1}$ is the processed noise vector.

The purpose of the digital BF step is to maximize the SINR when the digital BF is designed. To do this, an optimization problem can be formulated as follows:

$$\mathcal{P}3 : \max_{\mathbf{F}} \ \gamma_i \tag{15a}$$

$$\text{s.t. } \|\mathbf{f}_i\|^2 = 1, \quad \forall i \in \mathcal{S}. \tag{15b}$$

To solve the above optimization problem, the objective function can first be simplified as follows. Let $\hat{\mathbf{H}}_i = [\bar{\mathbf{h}}_1, \ldots, \bar{\mathbf{h}}_{i-1}, \bar{\mathbf{h}}_{i+1}, \ldots, \bar{\mathbf{h}}_S] \in \mathbb{C}^{S\times S-1}$ be the extended effective channel matrix that excludes $\bar{\mathbf{h}}_i$. Thus, the SINR in (14) can be written as

$$\gamma_i = \frac{\mathbf{f}_i^H \bar{\mathbf{h}}_i \bar{\mathbf{h}}_i^H \mathbf{f}_i}{\mathbf{f}_i^H (\hat{\mathbf{H}}_i \hat{\mathbf{H}}_i^H + \frac{\sigma^2}{P}\mathbf{I}_S)\mathbf{f}_i}. \tag{16}$$

Equation (16) is a Rayleigh quotient form. According to the Rayleigh-Ritz quotient theorem [26], the upper bound of γ_i is

$$\gamma_i \leq \lambda_{max}(\bar{\mathbf{h}}_i \bar{\mathbf{h}}_i^H, \hat{\mathbf{H}}_i \hat{\mathbf{H}}_i^H + \frac{\sigma^2}{P}\mathbf{I}_S), \tag{17}$$

where $\lambda_{max}(\mathbf{A}, \mathbf{B})$ is the largest eigenvalue of the matrix pair $\mathbf{A}$ and $\mathbf{B}$.

If $\mathbf{f}_i$ is the eigenvector equivalent to the largest eigenvalue, then equality can occur. Optimal $\mathbf{f}_i$ can then be written as $\mathbf{f}_i = \text{eigenvector}(\bar{\mathbf{h}}_i \bar{\mathbf{h}}_i^H, \hat{\mathbf{H}}_i \hat{\mathbf{H}}_i^H + \frac{\sigma^2}{P}\mathbf{I}_S)$. Finally, the optimal $\mathbf{f}_i$ can be written as

$$\mathbf{f}_i = \text{eigenvector}((\hat{\mathbf{H}}_i \hat{\mathbf{H}}_i^H + \frac{\sigma^2}{P}\mathbf{I}_S)^{-1} \bar{\mathbf{h}}_i \bar{\mathbf{h}}_i^H). \tag{18}$$

The digital BF vector is then normalized, i.e., $\mathbf{f}_i = \frac{\mathbf{f}_i}{\|\mathbf{f}_i\|}$, because of the unit power constraint of digital BF.

Remark 1: The SINR maximization method used in the digital BF step requires only low-dimensional effective CSI. Therefore, computational complexity can be reduced significantly. Furthermore, the SINR maximization method allows the digital BF design used above to attain a higher sum rate than designs that use ZF digital BF.

IV. Performance Analysis of the User Selection Algorithm

The proposed user selection algorithm finds an indirect solution by selecting users with the most spatial separation in order to maintain decent semi-orthogonality between the effective channel vectors. Hence, the sum-rate performance for digital BF is better than with a random selection. This section describes first the impact of effective channel vectors of two-user on user selection in multiuser MIMO systems with digital BF, such as the ZF method. This underlines the importance of instantaneous channels among the selected users being orthogonal. Then, we analyze the impact of angle correlation, beam patterns, and beamwidth on the proposed user selection algorithm and discuss its computational complexity.

A. Impact of Effective Channel Vectors of Two-User Using the ZF Method

This subsection investigates the impact of effective channel vectors on user selection when digital BF is adopted, using the ZF method, to mitigate multiuser interference. In the ZF method, to maximize the sum rate, the AP selects digital BF vectors $\mathbf{F}$ that can achieve the zero-interference condition $\sum_{j\neq i}^{S} \mathbf{f}_i^H \mathbf{H}_j = 0$. A common method to achieve zero interference is to use the pseudoinverse of the channel matrix of selected users in order to find the user that locally maximizes the total power projection. Finding the optimal solution to maximize the sum rate is challenging due to the computational complexity: it requires an exhaustive search over all K users. Thus, user selection that considers the channel state of the selected users is valuable.

We utilize the ZF method in this subsection for the sake of simplicity and traceability in the analysis. We will briefly review the relationship between the channel state of each selected user and the ZF digital BF technique, which nulls the effect of the other selected user by projecting the received signal in a direction orthogonal to that user. Following the same analysis as in [11], consider a simple example with two users with single antennas that transmit simultaneously to a two-antenna AP. x_1 and x_2 are the symbols concurrently transmitted by user$_1$ and user$_2$, respectively. The signal received at the AP is given by

$$\mathbf{r} = \mathbf{h}_1\ x_1 + \mathbf{h}_2\ x_2 + \mathbf{n}, \tag{19}$$

where $\mathbf{r} = [r_1, r_2]$ is the received vector at the AP, and $\mathbf{h}_1 = [h_{11}, h_{12}]$ and $\mathbf{h}_2 = [h_{21}, h_{22}]$ are the channels vectors of user$_1$ and user$_2$, respectively. $\mathbf{n} = [n_1, n_2]$ is the noise vector, where $n_1, n_2 \sim \mathcal{CN}(0, N_0)$, and N_0 is the noise power spectral density. We want to observe the effect of orthogonality and digital BF from the point of view of the SNR. Consider that the AP attempts to recover the symbol x_1. The interference from the other symbol x_2 can then be mitigated at the AP by projecting $\mathbf{r}$ in a direction orthogonal to $\mathbf{h}_2$. Then, the projected signal can be decoded. The estimate of x_1 is as follows:

$$\hat{x_1} = x_1 + \frac{h_{22}n_1 - h_{12}n_2}{h_{11}h_{22} - h_{21}h_{12}}. \tag{20}$$

By performing maximal-ratio combining [11], the SNR of x_1 when both symbols (x_1 and x_2) are transmitted simultaneously, denoted by SNR$_{Simult.}$, can be found as follows:

$$\begin{aligned} \text{SNR}_{Simult.} &= \frac{\mathbb{E}[\|x_1\|^2]}{\mathbb{E}[\|n_1\|^2]}, \\ &= \frac{\mathbb{E}[\|\mathbf{h}_1 x_1\|^2]}{N_0}\left(1 - \cos^2(\alpha)\right), \\ &= \text{SNR}_{prime}\left(1 - \cos^2(\alpha)\right), \end{aligned} \tag{21}$$

where SNR$_{prime}$ is the SNR of symbol x_1 when it is transmitted alone, and α is the Hermitian angle between the two channel vectors $\mathbf{h}_1$ and $\mathbf{h}_2$. This is defined as $0 \leq \alpha_H(\mathbf{h}_1, \mathbf{h}_2) \leq \pi/2$, such that

$$cos\alpha_H(\mathbf{h}_1, \mathbf{h}_2) = \frac{|\mathbf{h}_1 \cdot \mathbf{h}_2|}{\| \mathbf{h}_1 \| \| \mathbf{h}_2 \|}. \tag{22}$$

The Hermitian angle can be used to evaluate orthogonality and the spatial correlation between two channel vectors when non-orthogonal instantaneous channels among the selected users can result in multiuser interference [27], [28].

We can observe from the above example that the angle between the two channel vectors of user$_1$ and user$_2$ can affect the SNR$_{Simult.}$ when they transmit simultaneously. Fig. 5 shows the data-rate performance using (21) versus the angles between users for different SNR$_{prime}$ values. Higher performance can be achieved when the angle between users is nearly orthogonal. Hence, SNR$_{Simult.}$ depends on the angle between the two users as well as on the ZF technique.

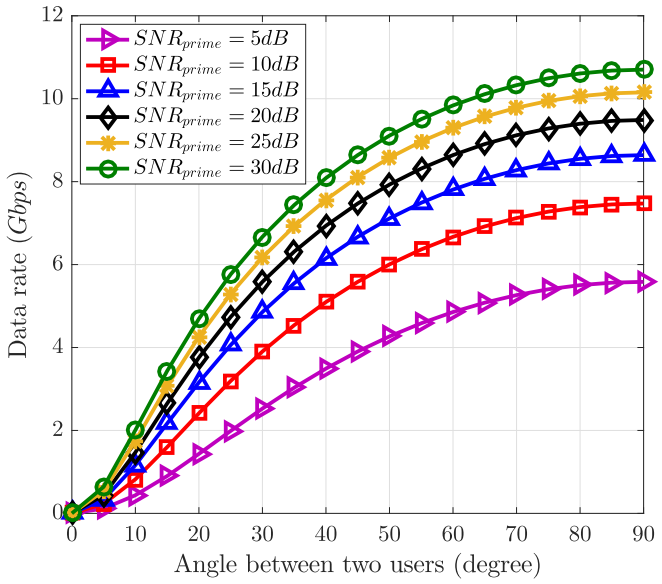

Fig. 5. Data-rate performance versus different angles between two users.

B. Impact of Angle Correlation on Proposed User Selection Algorithm

Angle correlation among the effective channel vectors of the selected users can affect the performance of the proposed algorithm after the digital BF stage. In order to justify the spatial separation or semi-orthogonality of the proposed user selection algorithm and analyze its benefit over the random user selection method, orthogonal vectors are first defined by adopting the ZF concept for traceability. Let $\boldsymbol{\beta}_a \in VG_{g1}$ or VG_{g2} (where $a = \{1, 2, ..., A\}$) be the semi-orthogonal vectors shown in Fig. 6(a). The orthogonal directions $\boldsymbol{\beta}_1$, $\boldsymbol{\beta}_3$, $\boldsymbol{\beta}_5$, and $\boldsymbol{\beta}_7$ represent the simultaneous selection among users for the first group VG_{g1}, while $\boldsymbol{\beta}_2$, $\boldsymbol{\beta}_4$, $\boldsymbol{\beta}_6$, and $\boldsymbol{\beta}_8$ are the equivalents for VG_{g2}.

Subsequently, $\boldsymbol{\beta}_a$ can be adopted to estimate if there are good spatial separations or alignments between $\boldsymbol{\beta}_a$ and each $\mathbf{h}_i$. This is accomplished by calculating the angles between the channel gain vectors of each user in either VG_{g1} or VG_{g2} with respect to $\boldsymbol{\beta}_a$. In other words, each user should be properly aligned with one of the defined semi-orthogonal vectors ($\boldsymbol{\beta}_a$) in order to maintain spatial separation. For example, as shown in Fig. 6(b), we can assume that user$_1$ ($\mathbf{h}_1$) and user$_4$ ($\mathbf{h}_4$) are nearly orthogonal to one another since they have the best alignment with $\boldsymbol{\beta}_1$ and $\boldsymbol{\beta}_2$, respectively. Thus, the semi-orthogonality selection criterion in the user selection algorithm allows better spatial separation and higher performance. Note that for generality, this analysis assumes that the beams focus only on one direction; the ULA beam pattern is neglected. The impact of the analog beam pattern is discussed in Subsection IV-C.

Proposition 1: A higher SINR and better spatial correlation can be attained as long as the angle between two effective channel vectors is orthogonal or the selected users are nearly orthogonal (semi-orthogonal) to one another when the number of users is large. Thus, multiuser interference can be mitigated, and the sum rate can be improved.

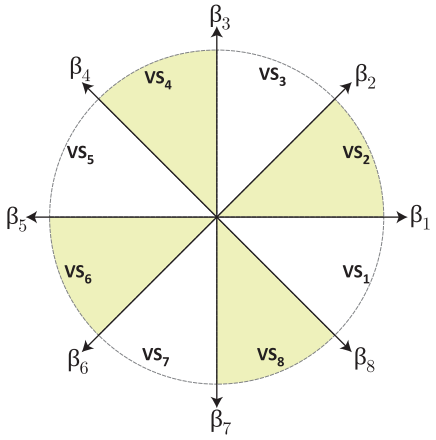

(a) $\boldsymbol{\beta}_a$, when $A = 8$.

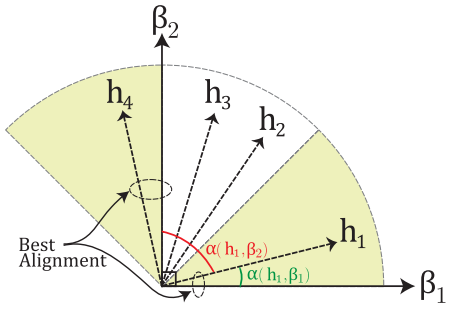

(b) Alignment metric example, when $A = 8$.

Fig. 6. User selection using the predefined orthogonal-direction vectors.

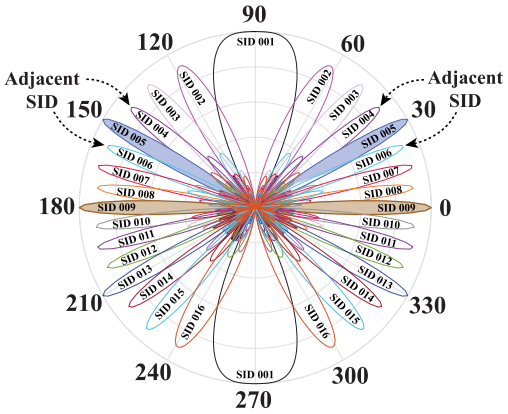

(a) Uniform linear array codebook.

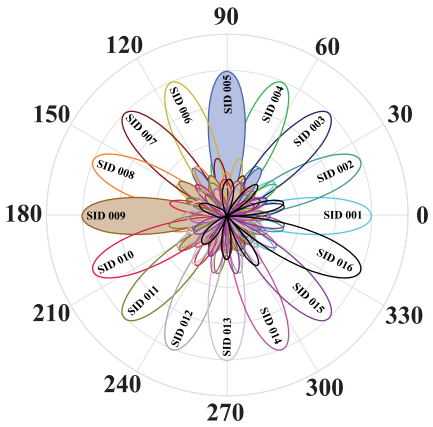

(b) Circular codebook.

Fig. 7. Antenna codebook beam patterns, where the number of beam patterns is 16.

Proof: Based on equation (14), the SINR of the i-th user can be written as

$$\gamma_i = \frac{|\mathbf{f}_i^H \bar{\mathbf{h}}_i|^2}{\sum_{j\neq i}^{S} |\mathbf{f}_i^H \bar{\mathbf{h}}_j|^2 + \frac{\sigma^2}{P}} = \frac{||\bar{\mathbf{h}}_i||^2 |\mathbf{f}_i^H \tilde{\mathbf{h}}_i|^2}{\sum_{j\neq i}^{S} ||\bar{\mathbf{h}}_j||^2 |\mathbf{f}_i^H \tilde{\mathbf{h}}_j|^2 + \frac{\sigma^2}{P}}, \tag{23}$$

where $\tilde{\mathbf{h}}_i = \frac{\bar{\mathbf{h}}_i}{||\bar{\mathbf{h}}_i||}$, a unit vector of the effective channel vector $\bar{\mathbf{h}}_i$. The first term in the denominator represents interference from the other $S-1$ selected users, and the second term denotes the noise.

Let ϑ denote the angle between $\mathbf{f}_i$ and $\bar{\mathbf{h}}_i$. Here, $\mathbf{f}_i$ can be decomposed as [27]

$$\mathbf{f}_i = (\cos\vartheta)\tilde{\mathbf{h}}_i + (\sin\vartheta)\mathbf{g}_i, \tag{24}$$

where $\mathbf{g}_i$ is a unit vector orthogonal to $\tilde{\mathbf{h}}_i$. Note we do not consider the detailed BF scheme for $\mathbf{f}_i$. Hence, the following analysis can be applied in various BF schemes.

Substituting (24) into (23), the SINR can be written as

$$\begin{aligned}\gamma_i &= \frac{||\bar{\mathbf{h}}_i||^2 \ \cos\vartheta^2}{\sum_{j\neq i}^{S} ||\bar{\mathbf{h}}_j||^2 \left|\left((\cos\vartheta)\ \tilde{\mathbf{h}}_i^H + (\sin\vartheta)\ \mathbf{g}_i^H\right)\tilde{\mathbf{h}}_j\right|^2 + \frac{\sigma^2}{P}} \\ &= \frac{||\bar{\mathbf{h}}_i||^2 \ \cos\vartheta^2}{\sum_{j\neq i}^{S} ||\bar{\mathbf{h}}_j||^2 \left|(\cos\vartheta)\ \tilde{\mathbf{h}}_i^H\tilde{\mathbf{h}}_j + (\sin\vartheta)\ \mathbf{g}_i^H\tilde{\mathbf{h}}_j\right|^2 + \frac{\sigma^2}{P}} \\ &= \frac{||\bar{\mathbf{h}}_i||^2 \ \cos\vartheta^2}{\sum_{j\neq i}^{S} ||\bar{\mathbf{h}}_j||^2 \left|(\cos\vartheta)\cos\alpha_{i,j} + (\sin\vartheta)\ \mathbf{g}_i^H\tilde{\mathbf{h}}_j\right|^2 + \frac{\sigma^2}{P}},\end{aligned} \tag{25}$$

where the last step is obtained from $\cos\alpha_{i,j} = \tilde{\mathbf{h}}_i^H\tilde{\mathbf{h}}_j$, and $\alpha_{i,j}$ denotes the angle between the two effective channel vectors $\bar{\mathbf{h}}_i$ and $\tilde{\mathbf{h}}_j$. The above equation indicates that the SINR depends on the angles between the two effective channel vectors. If the angle $(\alpha_{i,j})$ is small, i.e., close to 0, the interference can be significant because $\cos\alpha_{i,j}$ is large, and the SINR can thus be reduced. To enhance the SINR, we need to select users such that the angles between channel vectors are semi-orthogonal. ■

C. Impact of Beam Patterns on Proposed User Selection Algorithm

The analog beam patterns considered can affect the performance of the proposed user selection algorithm. In this subsection, we analyze the impact of the analog beam pattern of the ULA on the algorithm. As shown in Fig. 7(a), the analog beam pattern of the ULA is symmetrical with respect to the y-axis; there is an extra beam direction for each desired beam direction. This can affect the performance of the proposed user selection algorithm. For example, from Fig. 7(a), if SID 009 is selected for both user 1 and user 2, at 0° and 180°, respectively, then the beam separation is zero, which does not lead to orthogonal vectors. In addition, if SID 009 is selected for user 1 and either SID 008 or SID 010 is selected for user 2 at a mirror-opposite position (0° or 180°), this can

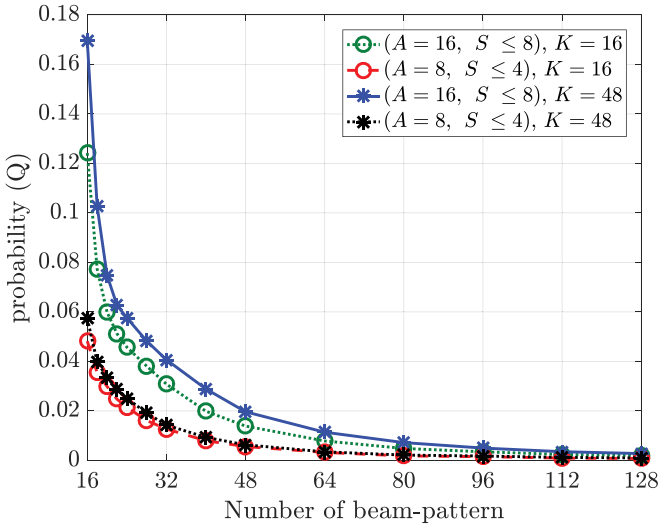

Fig. 8. The probability (Q) for different numbers of beam patterns.

lead to minimal SID separation, and semi-orthogonality is not maintained. The same result holds for other beam patterns, such as SID 005.

Although the ULA can affect the performance of the proposed user selection, the probability (Q) of two selected users being simultaneously located at mirror-opposite positions or of one of the selected users being located at an SIDs adjacent to the other is very low when the number of beam patterns is large. Fig. 8 shows this probability (Q) for different numbers of beam patterns using the ULA. It can be seen that Q is very low for all scenarios where $A = 16$, $A = 8$, $K = 48$, and $K = 16$, and is almost zero when the number of beam patterns is 128. Therefore, the performance analysis and evaluation of the proposed user selection algorithm and overall-HBF algorithm here and in Section V will not be affected as long as the number of beam patterns considered is sufficiently large.

In general, while the proposed overall-HBF algorithm can operate in any codebook, performance depends on the analog beam pattern considered. Other predefined RF codebooks, such as the circular codebook [29], can be considered for future work in order to evaluate and compare algorithm performance. As shown in Fig. 7(b), the circular antenna array has beams that only focus on one direction, unlike the ULA [29]. In addition, the proposed user selection algorithm can be extended for future work to add a selection criterion that depends on the beam-pattern (separation of SIDs) at the AP.

D. Impact of Beamwidth on Proposed User Selection Algorithm

The beamwidth of the beam pattern under consideration can influence the performance of the user selection algorithm or the spatial multiplexing gain. We aim to analyze the latter from the beamwidth point of view, defining it as the number or ratio of available, successful concurrent links after determining the SINR by eliminating interfering links. Since we are studying the effect of beamwidth on the user selection algorithm, we also consider a circular array and approximate it with a sectored, flat-top directional antenna model for simplicity and generality. This model is considered a useful idealization in interference analysis [30], [31]. Let $G(\theta, \phi)$ be the power gain antenna pattern of the directional antenna, where ϕ and θ are the azimuth and elevation angles, respectively. By assuming a horizontal plane, the directional antenna model is given by $g(\phi) = \frac{G(0,\phi)}{G_{max}}$, where $G_{max} = \max_{\phi} G(\phi)$. Then the sectored flat-top directional antenna model can be represented as

$$g(\phi) = \begin{cases} 1, & |\phi| \leq \frac{\Delta\phi}{2} \\ 0, & otherwise \end{cases} \tag{26}$$

where $\Delta\phi$ is the beam angle. The impact of the beamwidth of the user selection algorithm can be evaluated by measuring the SINR for each selected user in order to analyze the spatial multiplexing gain. Let P_{tx}, G_{tx}, G_{rx}, D, and n be the transmit power, transmitter antenna gain, receiver antenna gain, transmission distance, and path loss exponent, respectively. Then, from the *Friis* transmission formula, the power of the received signal for the i-th user is given by

$$P_{rx,i} = P_{tx,i} G_{max}^2(\phi_i) \left(\frac{\lambda}{4\pi}\right)^2 D_i^{-n}, \tag{27}$$

where $G_{max} = G_{tx} = G_{rx}$ is defined as the maximum antenna gain [30]. The SINR can then be written as

$$\gamma_i = \frac{P_{tx,i} G_{max}^2(\phi_i) \left(\frac{\lambda}{4\pi}\right)^2 D_i^{-n}}{\sum_{j \neq i} P_{tx,i} G_{max}^2(\phi_j) \left(\frac{\lambda}{4\pi}\right)^2 D_j^{-n} + N_o B_w} \tag{28}$$

where B_w and N_o are the system bandwidth and background noise power density, respectively.

Fig. 9 shows the impact of beamwidth using spatial multiplexing gain and average data rate of the proposed user selection algorithm for various beamwidths. The beamwidth and antenna directivity are evaluated using the SINR in (28). It can be seen that average data-rate performance decreases when the beamwidth increases due to the interference. Furthermore, we can see that when beamwidths are narrow (e.g., below $45°$), the user selection algorithm attains higher spatial multiplexing gain than when they are wider. The figure also shows that there is a slight degradation in performance when using the ULA antenna model due to the effect of the analog beam pattern of the ULA, as discussed in Subsection IV-C. Higher performance can be achieved when the number of VSs is large ($A = 16$), due to the increased number of simultaneous users. Nevertheless, a trade-off exists between performance and beamwidth. Thus, better sum-rate performance can be attained as long as the latter is kept sufficiently narrow.

E. Complexity Analysis of the User Selection

This subsection analyzes the computational complexity of the proposed user selection algorithm. To select a subset of users that locally maximizes the sum-power projection and hence grants zero interference, an exhaustive search is needed over a discrete set of size $\binom{K}{S}$ to find the optimal solution. The size and computation of the search space are

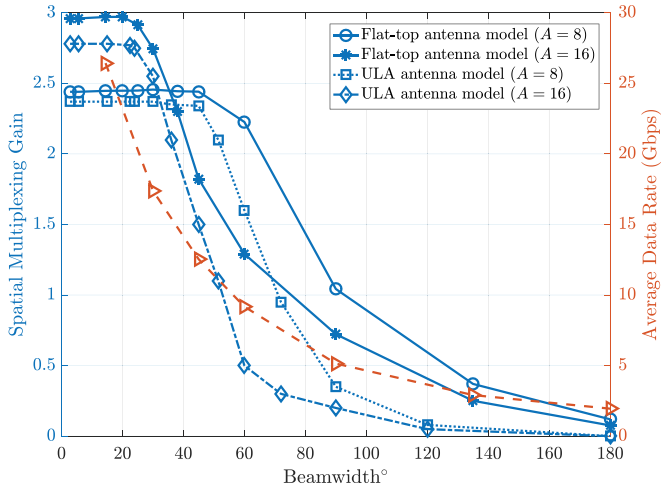

Fig. 9. User selection performance for various beamwidths.

prohibitively complex since mmWave propagation characteristics make a large number of antenna elements essential for mmWave communication. A large number of users (K) can also increase complexity since dense wireless networks are predicted in the near future. Therefore, the computational complexity of the optimal user selection solution is given by $\mathcal{O}(K^S)$, a polynomial complexity [32]. However, a sub-optimal user selection solution is exploited by utilizing orthogonality as a selection metric. The computational complexity of the user selection of our proposed overall-HBF algorithm is hence reduced to $\mathcal{O}(A)$. In addition, the proposed user selection algorithm does not require collecting the perfect CSI for user selection. Traditional user selection methods in multiuser MIMO systems, including optimal and sub-optimal schemes, do require this, thus creating significant overhead.

V. Performance Evaluation and Simulation Results

In this section, we conduct simulations to evaluate the performance of the proposed overall-HBF algorithm. First, the simulation set-up is introduced. Next, we evaluate the proposed algorithm with an optimal set of users in a simplified scenario. We then evaluate the average sum-rate performance of the proposed algorithm versus existing HBF algorithms. We also evaluate the energy efficiency performance of the proposed algorithm at the AP.

A. Simulation Set-Up

A Monte-Carlo simulation evaluates the proposed overall-HBF algorithm 50,000 times (simulating more than 2,000,000 BIs). For simplicity, our simulations do not account for the contention limitation of A-BFT; active users are assumed to always be available during A-BFT in every BI. The main performance criteria of this evaluation are the achievable sum rate of the selected users and the energy efficiency. The simulations adopt the channel model defined in [33], [34], a large-scale channel fading given by

$$PL(dB) = 20\log_{10}\left(\frac{4\pi D_0}{\lambda}\right) + 10n\log_{10}\left(\frac{D}{D_0}\right), \quad (29)$$

TABLE II
Simulation Parameters

Parameters	Value
Virtual sectors (A)	[8, 16]
Number of users (K)	8-64
AP antennas (N_r)	32-128
User antennas (N_t)	8-16
NLOS hall (n)	3.01
LOS hall (n)	2.17
LOS corridor (n)	1.64
Noise power spectral density (N_0)	-134 dBm/MHz
System bandwidth	2.16 GHz
Central frequency (f)	60 GHz

where D_0, D, and n are the free space reference distance, the propagation distance, and the path loss exponent, respectively. Note that (29) holds for $D \geq D_0$, and (29) is used to obtain the channel gain ($g_{i,l}$) in (3). The channels are single-path, and the locations of users are randomly distributed in $[0, 2\pi]$. Based on the location information of the i-th user and AP, the angle of arrival θ_i and the angle of departure ϕ_i can be obtained. In this way, the channel matrix $\mathbf{H}_i$ between the i-th user and AP can be constructed. In this simulation, we consider various application scenarios, such as non-line-of-sight (NLOS) in a hall, line-of-sight (LOS) in a hall, and LOS in a corridor, based on the measurements of the mmWave indoor environment [35]. Table II summarizes the simulation set-up parameters used to derive the performance results. We use MATLAB software for the numerical analysis, executed on a computer with an Intel Core i7-8559U CPU and 32GB random access memory (RAM). The operating system is Windows 10.

We compare the proposed overall-HBF algorithm with an optimal set of users and the analog BF of the IEEE 802.11ad standard, denoted by HBF-Full-Search and Analog-BF, respectively. We also compare the existing HBF algorithms that employ the ZF method and do not consider the user selection algorithm (random selection) when the user population is large, such as [17], [20], [21] and [22]. For ease of representation, the existing HBF algorithm is denoted by HBF-Random.

B. Optimal Set of Users: Performance and Complexity Comparison

Our aim in this subsection is to benchmark the performance of the proposed overall-HBF algorithm in a simplified scenario against both HBF-Full-Search and Analog-BF. We also include HBF-Random in the performance comparison. The average user rate versus the number of users is shown in Fig. 10. We can see from this figure that HBF-Random is clearly outperformed by HBF-Full-Search, overall-HBF, and Analog-BF in both situations when $N_r = 64$, $N_t = 16$ and $N_r = 16$, $N_t = 8$. It can also be seen that HBF-Full-Search achieves the highest performance, as expected, at the cost of computational complexity. This performance

TABLE III
SIMULATION TIME IN EACH RUN IN SECONDS

Number of users (K)	Overall-HBF $A = 8$, $S \leq 4$	Overall-HBF $A = 16$, $S \leq 8$	HBF-Full-Search $S = 4$	HBF-Full-Search $S = 8$
8	0.19	0.19	0.29	0.17
16	0.21	0.21	2.10	32.05
24	0.22	0.22	11.23	1878.81
32	0.22	0.22	36.83	26062.27
40	0.22	0.22	93.16	203285.67 (2.35 days)
48	0.23	0.23	197.69	880930.79 (10.2 days)
56	0.23	0.23	372.15	not available
64	0.23	0.23	648.11	not available

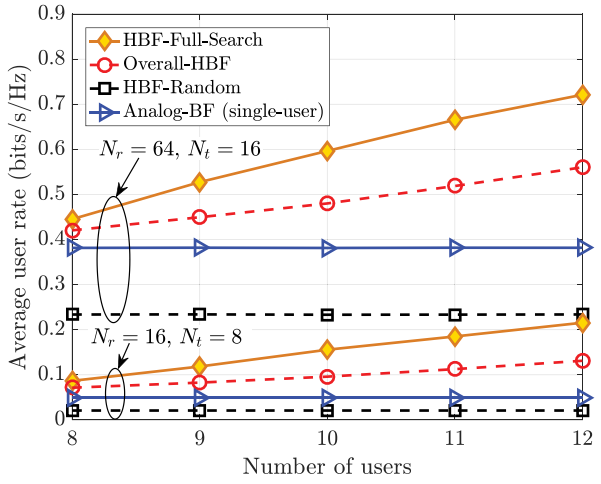

Fig. 10. Average user rate versus the number of users ($n = 2.17$, SNR $= 30$ dB, $S \leq 4$, $N_f = S$).

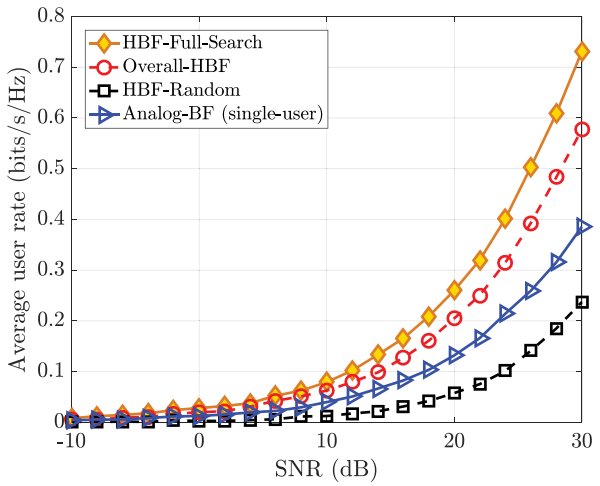

Fig. 11. Average user rate versus the SNR ($K = 12$, $n = 2.17$, $N_r = 64$ $S \leq 4$, $N_f = S$).

gap is sacrificed for the low complexity of the proposed user selection algorithm. For example, for $K = 12$, $N_r = 64$, and $N_t = 16$, the proposed algorithm can achieve nearly 80% of the performance of HBF-Full-Search while performing much better than HBF-Random.

In Fig. 11, we show the average user rate versus SNR when $K = 12$. The proposed overall-HBF outperforms HBF-Random because of the proposed user selection algorithm and the SINR maximization approach used in digital BF. As expected, the user rate increases exponentially when SNR increases; better performance can be realized when the SNR is high. As with Fig. 10, HBF-Full-Search achieves the highest performance while HBF-Random has the lowest.

In Table III, we illustrate the simulation time for each run in seconds. The simulation time of HBF-Full-Search is much higher than that of the proposed overall-HBF algorithm, and it increases significantly when the number of users increases. The simulation time becomes unfeasible, considering the capabilities of the device used, when the number of users is greater than 48 and $S = 8$. With these parameters, simulation time for HBF-Full-Search is more than 10 days, and up to 133 days, while the simulation time for the proposed algorithm is almost the same in all cases. Thus, the simulation time for the proposed algorithm is not affected by the increased number of users in our experiments.

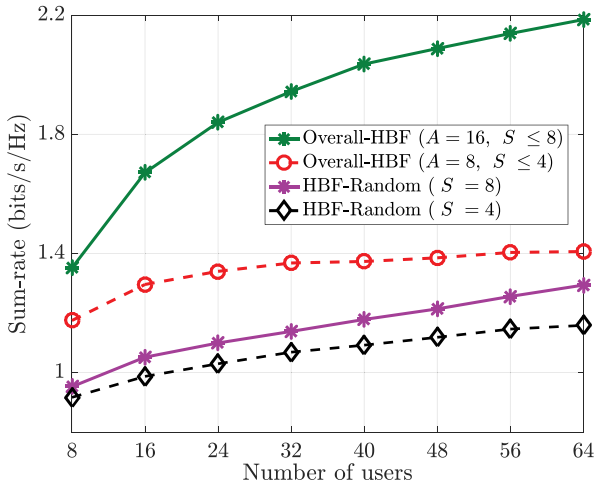

Fig. 12. Sum rate versus the number of users ($N_r = 64$, $N_t = 16$, $n = 2.17$ SNR $= 30$ dB, $N_f = S$).

C. Average Sum-Rate Performance

In this subsection, we compare the proposed overall-HBF with HBF-Random when $A = 16$ and $A = 8$. Different numbers of users are simulated in order to demonstrate the sum-rate performance in dense-deployment scenarios, as shown in Fig. 12. The proposed overall-HBF outperforms HBF-Random in both scenarios when the selected users are $S \leq 8$

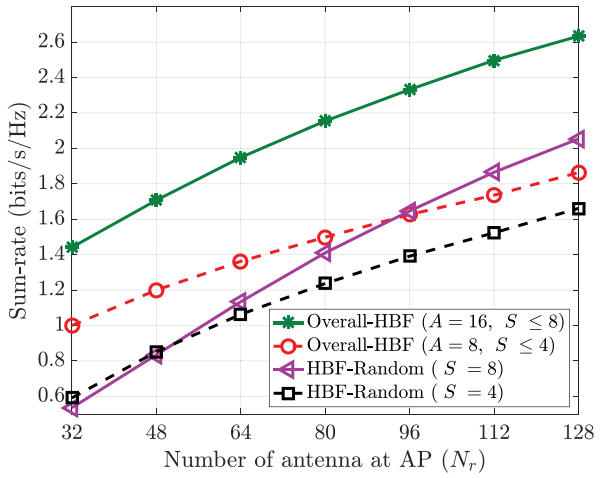

Fig. 13. Sum rate versus the number of AP['s] antennas ($K = 32$, $N_t = 16$, $n = 2.17$ SNR $= 30$ dB, $N_f = S$).

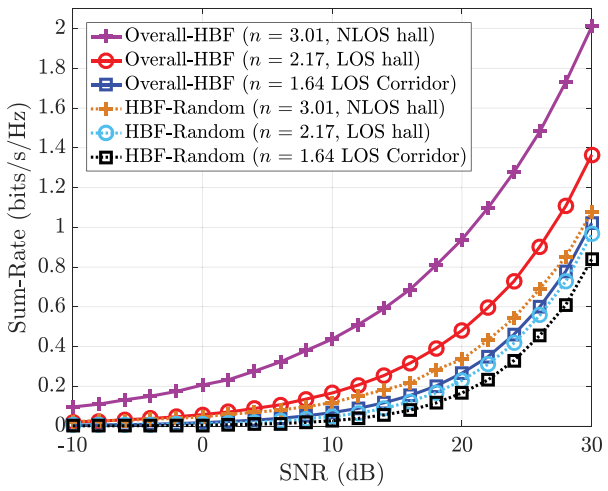

Fig. 14. Sum rate versus SNR in different scenarios ($K = 32$, $S \leq 4$, $N_r = 64$, $N_t = 16$, $N_f = S$).

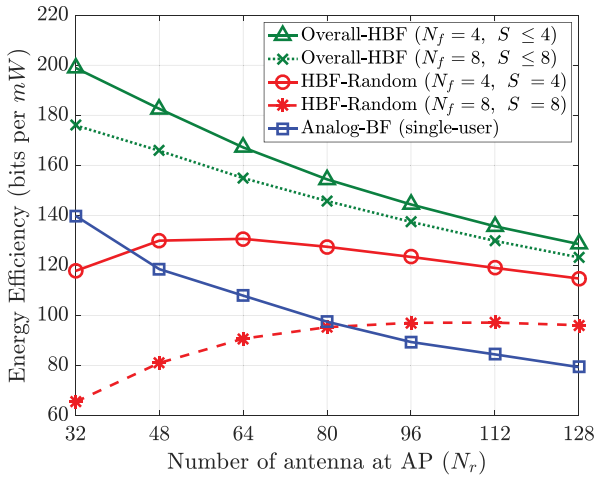

Fig. 15. Energy efficiency performance at the AP versus the number of antennas ($K = 32$, $N_t = 16$, $n = 2.17$ SNR $= 30$ dB).

and $S \leq 4$, and the sum-rate performance increases as K increases. Thus, higher performance can be achieved when K is large due to the higher probability of selecting users in the VG groups of the proposed user selection algorithm. Furthermore, a higher sum rate is obtained when $A = 16$ due to the higher spatial multiplexing gain, as discussed in Subsection IV-D.

Fig. 13 shows the impact of the number of antennas at the AP on sum-rate performance when $K = 32$. The proposed overall-HBF algorithm is compared with HBF-Random by considering both scenarios: when $S \leq 8$ and when $S \leq 4$. This figure shows that the proposed overall-HBF obtains the highest sum-rate performance, which increases as N_r increases. Furthermore, a higher sum-rate can also be obtained when the total number of VSs is 16, because of the spatial multiplexing gain.

In Fig. 14, we consider various path loss exponent scenarios based on mmWave measurements [35] in order to evaluate the sum-rate performance of our proposed overall-HBF algorithm versus SNR when $K = 32$ and $S \leq 4$. The proposed algorithm can achieve higher sum-rate performance than HBF-Random even with low SNR values due to the proposed user selection algorithm and the SINR maximization approach used in digital BF.

D. Energy Efficiency Performance

This subsection analyzes the energy efficiency performance of the proposed overall-HBF algorithm at the AP to demonstrate the impact of the power consumption of the analog-digital signal processing components of the HBF approach. The digital signal processing of the receiver components can consume a great deal of power due to the large number of antenna elements used in mmWave communication systems. Using a similar analytical approach as in [20] and [36], energy efficiency is defined as

$$E_{eff.} = \frac{R_{sum}}{P_{total}}, \tag{30}$$

where P_{total} is the total power consumption of the mmWave system at the AP. In order to compare total power consumption between HBF and analog BF, P_{total} represents the total power consumption at the AP of the HBF architecture approach (P_{total}^{HBF}) or of the analog-only BF architecture approach (P_{total}^{ABF}).

$$P_{total}^{HBF} = N_f(P_1 + P_2 + P_4) + P_3 + P_5 \tag{31}$$

$$P_{total}^{ABF} = P_1 + P_2 + P_3 + P_4 \tag{32}$$

where $P_1 = P_C + 2P_{ADC}$ denotes the total power consumption in the baseband receiver, $P_2 = P_M + P_{LO} + P_{LPF} + P_{PA}$ denotes the total power consumption of each RF chain, $P_3 = N_r(P_{LNA})$ denotes the total power consumption of the low noise amplifiers (LNAs), $P_4 = N_r(P_{PS})$ denotes the total power consumption of the analog phase shifters, and $P_5 = N_r(P_S)$ denotes the total power consumption of the splitters. The power consumption components and their values are given in Table IV [36]–[42].

In Fig. 15 and Fig. 16, the energy efficiency performance at the AP is shown by comparing the proposed overall-HBF algorithm, HBF-Random, and Analog-BF. Fig. 15 shows energy efficiency versus the number of antennas (N_r) when $N_f = 4$ and $N_f = 8$ at SNR $= 30$ dB. We can see

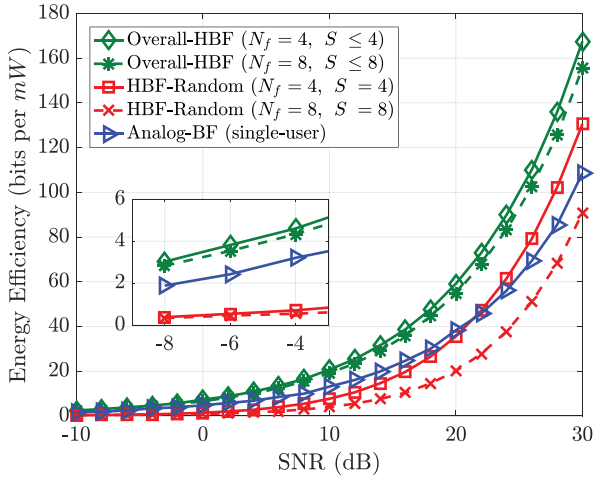

Fig. 16. Energy efficiency performance at the AP versus the SNR ($K = 32$, $N_r = 64$, $N_t = 16$, $n = 2.17$).

TABLE IV
POWER CONSUMPTION OF THE HBF AND ANALOG BF ARCHITECTURE COMPONENTS

Component	Notation	Value
Combiner	P_C	19.5 mW
ADC	P_{ADC}	200 mW
Mixer	P_M	16.8 mW
Local oscillator	P_{LO}	5 mW
Low pass filter	P_{LPF}	14 mW
Power amplifier	P_{PA}	5 mW
Low noise amplifier	P_{LNA}	39 mW
Splitter	P_S	19.5 mW
Phase shifter	P_{PS}	10 mW

that the proposed overall-HBF algorithm outperforms both HBF-Random and analog BF. In addition, the analog BF offers higher energy efficiency than HBF-Random when the number of antennas (N_r) is small, since it only uses one RF chain. However, as N_r increases, the energy efficiency of analog BF decreases, and it offers the lowest energy efficiency when $N_r > 96$. It is worth noting that the number of RF chains and the number of antennas at the AP can impact energy efficiency as well as the SNR. Even though Analog-BF is independent of N_f, the proposed overall-HBF algorithm offers higher energy efficiency for both lower and higher SNRs, as shown in Fig. 16. Another observation from both Fig. 15 and Fig. 16 is that HBF-Random offers lower energy efficiency, especially in the low SNR region, where the interference mitigation of the ZF method comes at the cost of energy efficiency.

VI. CONCLUSION

In this paper, we have proposed a novel overall-HBF algorithm that incorporates user selection for uplink multi-user MIMO mmWave WLANs. A subset of users can be selected using semi-orthogonality, and the remaining interference among selected users can be canceled by optimizing the digital BF. Theoretical analysis shows that the computational complexity of the proposed algorithm can be reduced significantly. Simulation results show that the proposed overall-HBF algorithm can outperform existing solutions in terms of both average sum rate and energy efficiency. Even though the proposed algorithm is based on the IEEE 802.11ay, it can be generalized to work in other mmWave communication systems (e.g., 5G) that utilize analog BF and digital BF. Future work will investigate the inter-cell interference problem for the uplink multiuser MIMO mmWave scenario when several hops have overlapping coverage by considering a clustering mechanism between a group of APs in a centralized or decentralized manner.

REFERENCES

[1] K. Aldubaikhy, W. Wu, and X. Shen, "HBF-PDVG: Hybrid beamforming and user selection for UL MU-MIMO mmWave systems," in *Proc. IEEE Globecom Workshops (GC Wkshps)*, Dec. 2018, pp. 1–6.
[2] P. Zhou *et al.*, "IEEE 802.11ay-based mmWave WLANs: Design challenges and solutions," *IEEE Commun. Surveys Tuts.*, vol. 20, no. 3, pp. 1654–1681, Mar. 2018.
[3] T. S. Rappaport *et al.*, "Millimeter wave mobile communications for 5G cellular: It will work!" *IEEE Access*, vol. 1, pp. 335–349, 2013.
[4] R. W. Heath, Jr., N. Gonzalez-Prelcic, S. Rangan, W. Roh, and A. M. Sayeed, "An overview of signal processing techniques for millimeter wave MIMO systems," *IEEE J. Sel. Top. Signal Process.*, vol. 10, no. 3, pp. 436–453, Apr. 2016.
[5] K. Aldubaikhy and X. Shen, "Simultaneous DL transmission in mmWave ultra dense networks: Inter-BSS interference prospective," in *Proc. IEEE Int. Conf. Commun. Workshops (ICC Workshops)*, May 2018, pp. 1–6.
[6] X. Shen *et al.*, "Methods and systems for multi-user beamforming," U.S. Patent Appl. 15 360 852, Nov. 23, 2016.
[7] N. Anand, J. Lee, S.-J. Lee, and E. W. Knightly, "Mode and user selection for multi-user MIMO WLANs without CSI," in *Proc. IEEE Conf. Comput. Commun. (INFOCOM)*, Apr. 2015, pp. 451–459.
[8] X. Xie and X. Zhang, "Scalable user selection for MU-MIMO networks," in *Proc. IEEE INFOCOM-IEEE Conf. Comput. Commun.*, Apr. 2014, pp. 808–816.
[9] T. Yoo and A. Goldsmith, "On the optimality of multiantenna broadcast scheduling using zero-forcing beamforming," *IEEE J. Select. Areas Commun.*, vol. 24, no. 3, pp. 528–541, Mar. 2006.
[10] W.-L. Shen, K. C.-J. Lin, S. Gollakota, and M.-S. Chen, "Rate adaptation for 802.11 multiuser MIMO networks," *IEEE Trans. Mobile Comput.*, vol. 13, no. 1, pp. 35–47, Jan. 2014.
[11] D. Tse and P. Viswanath, *Fundamentals of Wireless Communications*. Cambridge, U.K.: Cambridge Univ. Press, 2005.
[12] A. Zhou, T. Wei, X. Zhang, M. Liu, and Z. Li, "Signpost: Scalable MU-MIMO signaling with zero CSI feedback," in *Proc. 16th ACM Int. Symp. Mobile Ad Hoc Netw. Comput. (MobiHoc)*, Jun. 2015, pp. 327–336.
[13] C. Wang and R. Murch, "Adaptive downlink multi-user MIMO wireless systems for correlated channels with imperfect CSI," *IEEE Trans. Wireless Commun.*, vol. 5, no. 9, pp. 2435–2446, Sep. 2006.
[14] N. Czink, B. Bandemer, G. Vazquez-Vilar, L. Jalloul, C. Oestges, and A. Paulraj, "Spatial separation of multi-user MIMO channels," in *Proc. IEEE 20th Int. Symp. Pers., Indoor Mobile Radio Commun.*, Sep. 2009, pp. 1059–1063.
[15] K. Ko and J. Lee, "Low complexity multiuser MIMO scheduling with chordal distance," in *Proc. 42nd Annu. Conf. Inf. Sci. Syst.*, Mar. 2008, pp. 80–84.
[16] S. Kutty and D. Sen, "Beamforming for millimeter wave communications: An inclusive survey," *IEEE Commun.Surveys Tuts.*, vol. 18, no. 2, pp. 949–973, 2nd Quart. 2016.
[17] A. Alkhateeb, G. Leus, and R. W. Heath, Jr., "Limited feedback hybrid precoding for multi-user millimeter wave systems," *IEEE Trans. Wireless Commun.*, vol. 14, no. 11, pp. 6481–6494, Nov. 2015.
[18] O. E. Ayach, S. Rajagopal, S. Abu-Surra, Z. Pi, and R. W. Heath, Jr., "Spatially sparse precoding in millimeter wave MIMO systems," *IEEE Trans. Wireless Commun.*, vol. 13, no. 3, pp. 1499–1513, Mar. 2014.
[19] Z. Wang, M. Li, X. Tian, and Q. Liu, "Iterative hybrid precoder and combiner design for mmWave multiuser MIMO systems," *IEEE Commun. Lett.*, vol. 21, no. 7, pp. 1581–1584, Jul. 2017.
[20] X. Zhai, Y. Cai, Q. Shi, M. Zhao, G. Y. Li, and B. Champagne, "Joint transceiver design with antenna selection for large-scale MU-MIMO mmWave systems," *IEEE J. Sel. Areas Commun.*, vol. 35, no. 9, pp. 2085–2096, Sep. 2017.

[21] J. Choi, J. Mo, and R. W. Heath, Jr., "Near maximum-likelihood detector and channel estimator for uplink multiuser massive MIMO systems with one-bit ADCs," *IEEE Trans. Commun.*, vol. 64, no. 5, pp. 2005–2018, May 2016.

[22] J. Li, L. Xiao, X. Xu, and S. Zhou, "Robust and low complexity hybrid beamforming for uplink multiuser MmWave MIMO systems," *IEEE Commun. Lett.*, vol. 20, no. 6, pp. 1140–1143, Jun. 2016.

[23] *IEEE Draft Standard for Information Technology—Telecommunications and Information Exchange Between Systems Local and Metropolitan Area Networks—Specific Requirements—Part 11: Wireless LAN Medium Access Control (MAC) and Physical Layer (PHY) Specifications—Amendment: Enhanced Throughput for Operation in License-Exempt Bands Above 45 GHz*, IEEE Standard P802.11ay/D2.0, Jul. 2018.

[24] M. R. Akdeniz *et al.*, "Millimeter wave channel modeling and cellular capacity evaluation," *IEEE J. Sel. Areas Commun.*, vol. 32, no. 6, pp. 1164–1179, Jun. 2014.

[25] W. Wu, N. Cheng, N. Zhang, P. Yang, W. Zhuang, and X. Shen, "Fast mmWave beam alignment via correlated bandit learning," *IEEE Trans. Wireless Commun.*, vol. 18, no. 12, pp. 5894–5908, Dec. 2019, doi: 10.1109/TWC.2019.2940454.

[26] A. Tarighat, M. Sadek, and A. H. Sayed, "A multi user beamforming scheme for downlink MIMO channels based on maximizing signal-to-leakage ratios," in *Proc. IEEE Int. Conf. Acoust., Speech, Signal Process. (ICASSP)*, Mar. 2005, pp. 1129–1132.

[27] T. Yoo, N. Jindal, and A. Goldsmith, "Multi-antenna downlink channels with limited feedback and user selection," *IEEE J. Sel. Areas Commun.*, vol. 25, no. 7, pp. 1478–1491, Sep. 2007.

[28] K. Scharnhorst, "Angles in complex vector spaces," *Acta Applicandae Math.*, vol. 69, no. 1, pp. 95–103, Oct. 2001.

[29] W. Feng, Z. Xiao, D. Jin, and L. Zeng, "Circular-antenna-array-based codebook design and training method for 60 GHz beamforming," in *Proc. IEEE Wireless Commun. Netw. Conf. (WCNC)*, Apr. 2013, pp. 4140–4145.

[30] S. Singh, R. Mudumbai, and U. Madhow, "Interference analysis for highly directional 60-GHz mesh networks: The case for rethinking medium access control," *IEEE/ACM Trans. Netw.*, vol. 19, no. 5, pp. 1513–1527, Oct. 2011.

[31] J. Qiao, X. Shen, J. W. Mark, and Y. He, "MAC-layer concurrent beamforming protocol for indoor millimeter-wave networks," *IEEE Trans. Veh. Technol.*, vol. 64, no. 1, pp. 327–338, Jan. 2015.

[32] D. Gesbert, M. Kountouris, R. W. Heath, Jr., C.-B. Chae, and T. Salzer, "Shifting the MIMO paradigm," *IEEE Signal Process. Mag.*, vol. 24, no. 5, pp. 36–46, Sep. 2007.

[33] G. R. Maccartney and T. S. Rappaport, "Rural macrocell path loss models for millimeter wave wireless communications," *IEEE J. Sel. Areas Commun.*, vol. 35, no. 7, pp. 1663–1677, Jul. 2017.

[34] W. Wu, N. Zhang, N. Cheng, Y. Tang, K. Aldubaikhy, and X. Shen, "Beef up mmWave dense cellular networks with D2D-assisted cooperative edge caching," *IEEE Trans. Veh. Technol.*, vol. 68, no. 4, pp. 3890–3904, Apr. 2019.

[35] S. Geng, J. Kivinen, X. Zhao, and P. Vainikainen, "Millimeter-wave propagation channel characterization for short-range wireless communications," *IEEE Trans. Veh. Technol.*, vol. 58, no. 1, pp. 3–13, Jan. 2009.

[36] W. B. Abbas, F. Gomez-Cuba, and M. Zorzi, "Millimeter wave receiver efficiency: A comprehensive comparison of beamforming schemes with low resolution ADCs," *IEEE Trans. Wireless Commun.*, vol. 16, no. 12, pp. 8131–8146, Dec. 2017.

[37] R. Mendez-Rial, C. Rusu, N. Gonzalez-Prelcic, A. Alkhateeb, and R. W. Heath, Jr., "Hybrid MIMO architectures for millimeter wave communications: Phase shifters or switches?" *IEEE Access*, vol. 4, pp. 247–267, 2016.

[38] Y. Yu, P. G. M. Baltus, A. De Graauw, E. Van Der Heijden, C. S. Vaucher, and A. H. M. Van Roermund, "A 60 GHz phase shifter integrated with LNA and PA in 65 nm CMOS for phased array systems," *IEEE J. Solid-State Circuits*, vol. 45, no. 9, pp. 1697–1709, Sep. 2010.

[39] Y.-H. Lin and H. Wang, "A low phase and gain error passive phase shifter in 90 nm CMOS for 60 GHz phase array system application," in *IEEE MTT-S Int. Microw. Symp. Dig.*, May 2016, pp. 1–4.

[40] M. Kraemer, D. Dragomirescu, and R. Plana, "Design of a very low-power, low-cost 60 GHz receiver front-end implemented in 65 nm CMOS technology," *Int. J. Microw. Wireless Technol.*, vol. 3, no. 2, pp. 131–138, Mar. 2011.

[41] N. Deferm and P. Reynaert, *CMOS Front Ends for Millimeter Wave Wireless Communication Systems*. Cham, Switzerland: Springer, Jan. 2015. [Online]. Available: https://www.springer.com/gp/book/9783319139500

[42] R. Mendez-Rial, C. Rusu, N. Gonzalez-Prelcic, A. Alkhateeb, and R. W. Heath, Jr., "Hybrid MIMO architectures for millimeter wave communications: Phase shifters or switches?" *IEEE Access*, vol. 4, pp. 247–267, 2016.

Khalid Aldubaikhy (Student Member, IEEE) received the B.E. degree from Qassim University, Buraydah, Saudi Arabia, in 2008, the M.A.Sc. degree in electrical and computer engineering from Dalhousie University, Halifax, NS, Canada, in 2012, and the Ph.D. degree in electrical and computer engineering from the University of Waterloo, Waterloo, ON, Canada, in 2019. He is currently an Assistant Professor with Qassim University. His research interests include millimeter-wave wireless networks, medium access control, impulse radio ultra-wideband, and millimeter-wave 5G cellular networks.

Wen Wu (Student Member, IEEE) received the B.E. degree in information engineering from the South China University of Technology, Guangzhou, China, and the M.E. degree in electrical engineering from the University of Science and Technology of China, Hefei, China, in 2012 and 2015, respectively, and the Ph.D. degree in electrical and computer engineering from the University of Waterloo, Waterloo, ON, Canada, in 2019. Since 2019, he has been working as a Post-Doctoral Fellow with the Department of Electrical and Computer Engineering, University of Waterloo. His research interests include millimeter-wave networks and AI-empowered wireless networks.

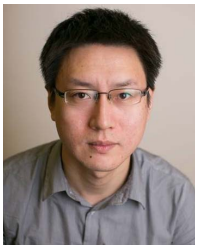

Qiang Ye (Member, IEEE) received the Ph.D. degree in electrical and computer engineering from the University of Waterloo, Waterloo, ON, Canada, in 2016. He was a Post-Doctoral Fellow with the Department of Electrical and Computer Engineering, University of Waterloo, from December 2016 to November 2018, where he was a Research Associate from December 2018 to September 2019. He has been an Assistant Professor with the Department of Electrical and Computer Engineering and Technology, Minnesota State University, Mankato, MN, USA, since September 2019. His current research interests include 5G networks, software-defined networking and network function virtualization, network slicing, artificial intelligence and machine learning for future networking, protocol design, and end-to-end performance analysis for the Internet of Things.

Xuemin (Sherman) Shen (Fellow, IEEE) received the Ph.D. degree in electrical engineering from Rutgers University, New Brunswick, NJ, USA, in 1990. He is currently a University Professor with the Department of Electrical and Computer Engineering, University of Waterloo, Waterloo, ON, Canada. His research focuses on resource management in interconnected wireless/wired networks, wireless network security, social networks, smart grid, and vehicular ad hoc and sensor networks. He is also a registered Professional Engineer of Ontario, Canada, an Engineering Institute of Canada Fellow, a Canadian Academy of Engineering Fellow, a Royal Society of Canada Fellow, and a Distinguished Lecturer of the IEEE Vehicular Technology Society and Communications Society. He received the Joseph LoCicero Award in 2015, the Education Award in 2017 from the IEEE Communications Society, the James Evans Avant Garde Award in 2018 from the IEEE Vehicular Technology Society, the Excellent Graduate Supervision Award in 2006, and the Outstanding Performance Award in 2004, 2007, 2010, and 2014 from the University of Waterloo and the Premier's Research Excellence Award (PREA) in 2003 from the Province of Ontario, Canada. He served as the Technical Program Committee Chair/Co-Chair for the IEEE Globecom'16, the IEEE Infocom'14, the IEEE VTC'10 Fall, the IEEE Globecom'07, the Symposia Chair for the IEEE ICC'10, the Tutorial Chair for the IEEE VTC'11 Spring, and the Chair for the IEEE Communications Society Technical Committee on Wireless Communications, and P2P Communications and Networking. He is the Editor-in-Chief of the IEEE INTERNET OF THINGS JOURNAL and the Vice President on Publications of the IEEE Communications Society.